Applied Catalysis B: Environmental 174–175 (2015) 367–375

Contents lists available at ScienceDirect

Applied Catalysis B: Environmental

journal homepage: www.elsevier.com/locate/apcatb

One step synthesis of N-doped and Au-loaded TiO_2 nanoparticles by laser pyrolysis: Application in photocatalysis

Sarah Bouhadoun[a], Chantal Guillard[b], Frédéric Dapozze[b], Sukhvir Singh[c], David Amans[d], Johann Bouclé[e], Nathalie Herlin-Boime[a,*]

[a] CEA, IRAMIS, NIMBE, CNRS UMR 3685, F-91191 Gif sur Yvette, France
[b] Institut de recherche sur la catalyse et l'environnement, IRCELYON, CNRS-University of Lyon, Villeurbannes 69100, France
[c] CSIR-National Physical Laboratory, Dr. K.S.Krishnan Marg, New Delhi 110012, India
[d] UMR5306CNRS, Institut Lumière Matière et Université Lyon 1, F-69622 Villeurbanne, France
[e] XLIM UMR 7252, Université de Limoges/CNRS, 87060 Limoges Cedex, France

ARTICLE INFO

Article history:
Received 6 January 2015
Received in revised form 9 March 2015
Accepted 14 March 2015
Available online 17 March 2015

Keywords:
Laser pyrolysis
Gold
N-doped TiO_2
Formic acid degradation
Visible light

ABSTRACT

Photocatalysis is a major tool for air and water depollution and photocatalysts with improved efficiency in the visible range are still needed. In this context, we show that N-TiO_2 nanoparticles modified with Au, called Au/N-TiO_2, seem to represent a good compromise: significant photocatalytic activity is observed under visible light together with an activity higher than TiO_2 P25 under UV irradiation. In order to demonstrate such efficiency of the Au/N-TiO_2 sample, TiO_2, Au-TiO_2, N-TiO_2 and Au modified N-TiO_2 nanoparticles were synthesized in one step using the laser pyrolysis method. The photocatalytic activity of the powders was evaluated through the photocatalytic degradation of formic acid (FA) both under UV and visible light irradiation. Under UV irradiation, all the laser-synthesized samples exhibit a high efficiency compared to commercial TiO_2 P25. Moreover, the modification by Au induces an enhancement of the photocatalytic activity compared to pure TiO_2 even at very low concentrations. Under visible light, the N-doped samples exhibit some photoactivity and the degradation rate of FA in presence of Au/N-TiO_2 is much increased compared to N-TiO_2. In conclusion, our Au/N-TiO_2 sample exhibits efficiency better than P25 under UV together with an activity under visible light.

1. Introduction

Since the discovery of its photocatalytic activity [1,2], titanium dioxide (TiO_2) remains the most widely used semiconductor owing to its applications in various fields such as environment (air and water purification), energy (water splitting, photovoltaic cells), medicine (cancer treatment, antibacterial), gas sensors and photocatalysis [3,4]. This material is very efficient due its properties: it presents strong oxidizing power [5], interesting optical-electronic properties [6], good photochemical stability, non-toxicity, and low cost. However, two mains limitations are encountered when using this material: its absorption is mainly located in the UV range which represents only 3–5% of the solar spectrum and its efficiency is limited by charge recombination after excitation. Therefore, many studies deal with gap engineering in order to shift it in the visible range and take advantage of this part of the solar light and/or enhancing charge separation by reducing the electron/hole recombination which is the major loss mechanism [7]. Indeed, modification of TiO_2 nanoparticles (NPs) surface with noble metal ions such as Pt, Ag, Pd and Au [8–11] allows increasing the photocatalytic efficiency. Concerning Au–TiO_2 NPs, a strong absorption of the visible light has also been reported thanks to surface resonance plasmon (SPR) of their free electrons [12,13]. Therefore, plasmonic photocatalyst Au–TiO_2 showed high efficiency in photoactivated reactions like acetic acid and 2-propanol degradation under both UV and visible irradiation [14], thiocyanate oxidation [15] and chemoselective oxidation of alcohols [16] with visible irradiation, CO_2 reduction with either UV (245, 365 nm), or visible (532 nm) [17], water splitting for H_2 and O_2 generation under UV and visible light [18,19]. The improvement of activity under UV light was attributed to the better interfacial charge transfer in presence of metallic NPs while the appearance of significant activity under visible irradiation was attributed to the SPR allowing absorption of visible light. This enhancement is explained in the literature by the two roles played by Au particles; on the one hand, the photoexcited electrons of gold surface plasmon can be injected to the

* Corresponding author at: Laboratoire édifices nanométriques (LEDNA), Nanosciences et Innovation pour les Matériaux, la Biomédecine et l'Energie (NIMBE), CEA Saclay, 91191 Gif/Yvette, France. Tel.: +33 1 69 08 36 84.
E-mail addresses: sarah.bouhadoun@cea.fr (S. Bouhadoun), nathalie.herlin@cea.fr (N. Herlin-Boime).

http://dx.doi.org/10.1016/j.apcatb.2015.03.022
0926-3373/

conduction band of TiO_2 creating separated electrons-holes and consequently increase their lifetime by reducing recombination [18], thus improve the photocatalytic activity. On the other hand, Au NPs can transfer electron from the TiO_2 surface to the adsorbed molecular oxygen. The size, shape, content and surrounding environment of gold nanoparticles can influence the SPR [14,20–24].

Another approach to extend the absorption of TiO_2 in the visible region is doping TiO_2 with ions like N, C, F, P or S [25,26]. Asahi et al. [27] have theoritically and experimentally studied the electronic structure of antase TiO_2 crystal doped with different atoms (C, F, S, P, N). Substitutional O^{2-} anions by these atoms gives rise to localized states within conduction and valence bands which narrows band gap [28]. In consequence, the presence of these non-metals elements in the lattice of TiO_2 gives rise to enhanced visible light activity. Nitrogen was reported as the most promising dopant [27,29]. Buzby et al. [30] and Shang et al. [31] showed that N-TiO_2 NPs increased visible light activity for the degradation of 2 and 4-chlorophenol, respectively.

However, the combination of these two effects (noble metal and nitrogen doping) has not been extensively studied. Tian et al. [32] and Wu et al. [33] synthesized Au/N-TiO_2 photocatalysts with much higher visible light activity when compared to single N-TiO_2 or Au-loaded TiO_2 for the degradation of 2-4,DCP and methyl orange respectively. Theoretical calculations [34] report that Au adsorption on TiO_2 surfaces significantly increase the amount of N implanted in the oxide and made it more active for the dissociation of water. A higher rate degradation of oxalic acid under UV–vis irradiation with gold modified N-TiO_2 photocatalysts was also reported [35]. Generally, most of the synthesis methods in the literature are made by the same methods, which need several steps, such as sol-gel process. For the modification by gold nanoparticles: the methods that are usually used are deposition-precipitation, impregnation, and photoreduction [3].

In the present paper, we report the one-step synthesis of TiO_2, N-TiO_2, and co-doped Au-N/TiO_2 nanoparticles with controlled size, composition, and good dispersion of metallic elements through the laser pyrolysis (LP) method. The main aim of this study was the evaluation of the influence of the co-doped gold and nitrogen on TiO_2 powders compared to TiO_2 reference sample synthesized in comparable conditions as well as to the literature reference TiO_2 Evonik P25®. In this study, gold nanoparticles were chosen, because of their great catalytic activity for different reactions [36,37]. The photocatalytic activity was tested by the decomposition of formic acid (FA) in aqueous solutions under both visible and UV irradiation under atmospheric conditions. The kinetic analysis and of the most active samples was determined.

2. Experimental methods

2.1. Chemicals

Titanium tetraisopropoxide (TTIP, 97% purity) and hydrogen tetrachloroaurate (III) $HAuCl_4{\cdot}3H_2O$ were respectively used as titanium and gold source for synthesis of TiO_2 and Au–TiO_2 nanoparticles. These reactants and the model pollutant HCOOH were obtained from Sigma-Aldrich and used without further purification. Absolute ethanol (≥99.99%) was purchased from Merck Millipore (Germany). Ammoniac NH_3 and Argon gases were supplied by Messer. Commercial reference P25 was obtained from Evonik.

2.2. Synthesis of photocatalysts

The laser pyrolysis method has already been described for the synthesis of TiO_2 nanoparticles [38,39]; briefly it is based on the absorption of the radiation of high power CO_2 Laser by a precursor. TTIP was used as precursor for the synthesis of TiO_2. For the synthesis of gold containing nanoparticles, the starting reagents are TTIP and $HAuCl_4{\cdot}3H_2O$. The preparation of these precursors consists in dissolving the appropriate amount of gold precursor (from 0.08 to 1.33 g) in 50 mL of absolute ethanol. 240 mL of TTIP were added gradually to the yellow resulting solution. The mixture was left under constant stirring for 10 min to ensure complete mixing. The procedure was performed under argon atmosphere in order to avoid hydrolysis of TTIP. The precursors were transferred to an ultrasonic spraying generator (Pyrosol model from RBI, France) where liquid droplets were formed, then an aerosol appeared. The droplets were carried out by a 700 $cm^3\ min^{-1}$ argon flow through a 6 mm diameter nozzle into the reaction zone where the interaction occurs with the laser beam. In order to ensure N doping, a flow of ammonia gas (100–250 $cm^3\ min^{-1}$) was added to the flow before entering the reaction zone. The pressure in the reactor was maintained constant at the atmospheric pressure (98.7 kPa). Powders were carried out of the reaction zone by argon flow and collected on filters.

Due to the presence of C in precursors, the obtained powders contain some Carbon removed by simple annealing at 400 °C under air flow (650 $cm^3\ min^{-1}$) in an oven (Pyrox). The heating rate was 20° C min^{-1} and the dwell time 3 h. It was checked that this annealing treatment does not significantly modify the crystalline phase. In the following parts, the samples containing gold will be labeled *X*–Au–TiO_2 where *X* is the gold amount (wt%) as measured by inductively coupled plasma optical emission spectrometry (ICP- OES). TiO_2 synthesized by laser pyrolysis will be labeled TiO_2 LP, while Nitrogen containing samples will be labeled N-TiO_2.

2.3. Characterization methods

The specific surface area (S_{BET}) was measured by nitrogen adsorption- desorption isotherms (Micromeritics Flowsorb II 2300 instrument) using the Brunauer–Emmett–Teller (BET) method. Prior to measurements, all samples were degassed at 150 °C for 1 h.

Gold content was measured by inductively coupled plasma optical emission spectrometry (ICP-OES) measurement (Horiba Jobin Yvon Activa) at IRCELYON.

Diffuse reflectance spectra (DRS) were measured in the range 200–800 nm using a Jasco V-572 UV–vis spectrophotometer equipped with diffuse reflectance sphere. The baseline was recorded using either barium sulfate or Spectralon reference. The band gap energies were deduced from the measurements according to the Kubelka–Munk theory.

For transmission electron microscopy (TEM) observations, the samples were prepared by sonicating for few minutes in ethanol, and then dropping one droplet of the suspension on copper coated carbon grids. The morphology and the crystallite size of the different powders were determined by a CM12 microscope at an accelerating voltage of 80 kV and high resolution TEM (HRTEM) using a FEI, model: Tecnai G2 F30 STWIN operated at 300 kV with a point resolution of 2.05 Å. Particle size distributions were determined by counting at least 80 particles with the Image J software.

2.4. Photocatalytic experiments

The photocatalytic efficiencies of samples were evaluated by following the degradation of formic acid (FA) (1086 $\mu mol\ L^{-1}$) in water. Formic acid was chosen as a model pollutant molecule because its mineralization occurs without any intermediate species [40]. Moreover, the curve showing the evolution of HCOOH concentration is superimposed to the disappearance curve of TOC (total organic carbon). The photocatalytic tests were carried out in a

Pyrex photoreactor. For UV irradiation, a mercury lamp Phillips HPK 125 W with optical filters 7.6 and 0.52 (Corning) were employed to obtain an emission peak centered at $\lambda = 365$ nm. The radiant flux at 4.2 mW cm^{-2} (7.7×10^{15} photons s^{-1} cm^{-2}) was measured using a VLX-3W radiometer with 365 nm sensor. The distance between the bottom of the reactor and the UV source is 2 cm. For visible light illumination in the region (400–800 nm), LED lamp was used; the photon flux was measured around 85×10^{-3} μmol s^{-1}. Both lamps were placed at the bottom of the reactor; the illuminated area was 12.5 cm^2. Circulating water between lamp and reactor maintain the solution temperature at 20 °C. Before irradiation, the system with TiO_2 concentration of 1 g L^{-1} was always stirred in the dark for 30 min. Such duration was proved sufficient to reach the adsorption-desorption equilibrium of formic acid on surfaces.

2.5. Analytical determination

At regular time intervals of irradiation, aliquots of FA suspensions were collected, filtered using 0.45 μm Millipore filters before analysis. The concentrations of FA remaining after adsorption and during the photocatalytic degradation process were determined using HPLC analysis. VARIAN Prostar HPLC apparatus equipped with a single wavelength UV–vis detector and a 300 mm × 7.8 mm carbohydrate analysis column (COREGEL-87H3) was used. The mobile phase was H_2SO_4 solution (5 10^{-3} mol L^{-1}) and the flow rate was fixed at 0.7 cm^3 min^{-1}. The detection wavelength was set at 210 nm.

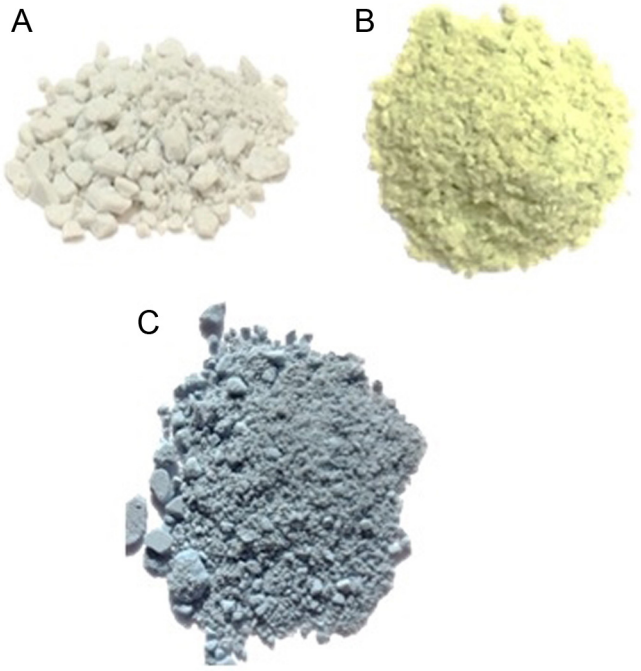

Fig. 1. Color evolution of typical (a) TiO_2 LP, (b) N-TiO_2 and (c) 0.16-Au–TiO_2, respectively after annealing treatment under air at 400 °C.

3. Results and discussion

3.1. Synthesis

The synthesis experiments were stopped after 80–90 min in order to collect sufficient amount of each sample for characterization and photocatalytic tests, i.e., about 1 g in the chosen experimental conditions. Table 1 presents the main experimental parameters and characterization results. The powders have different colors related to their composition: TiO_2 LP appears gray; Au modified photocatalysts appear from light blue to blue. The incorporation of nitrogen resulted in a dark blue color and Au/N-TiO_2 sample exhibits light green color (Fig. 1). As noted before, powders were annealed under air at 400 °C in order to remove residual carbon. After this treatment, the colors evolve from gray to white for pure TiO_2 and from dark blue to yellow for N modified TiO_2. *X*–Au–TiO_2 samples remain of blue color.

3.2. Characterizations

3.2.1. Morphology and structure

The morphology of a typical Au–TiO_2 sample is shown in Fig. 2A. The particles appear mainly of round shape with an average diameter of 7.5 nm, and are arranged in a chain like manner typical of gas phase synthesis. Pictures (not shown here) were recorded for all other samples, proving similar morphology. The mean size deduced from these pictures as well as BET and XRD measurements are given in Table 2. All these measurement are in good agreement with a crystallite diameter slightly smaller than grain size. Fig. 2B presents a typical HRTEM image of the 0.16-Au–TiO_2 sample. On this picture, several crystallites are present and pointed with different interplanar distance *d*. This distance was measured by counting the planes on the image (10 planes = 3.52 or 2.07 nm) corresponding to lattice fringe of (0 0 1) and (2 0 0) anatase TiO_2 and Au features respectively. FFT analysis was also performed with the same results on several particles and along several axes. Au NPs are of very small size (from 2 to 3 nm). From these NPs sizes (7.5 and 2 nm) and using materials density (3.2 and 19.3), the ratio between the number of TiO_2 and Au NPs can be estimated to 50 in the 0.16-Au–TiO_2 sample containing the highest Au amount. This estimation seems in good agreement with HRTEM pictures where few Au NPs could be identified. Specific surface areas measurements (table 2) show only a slight difference between the different samples TiO_2 LP, N-TiO_2, *X*–Au–TiO_2 and Au/N-TiO_2. These measurements show that the specific surface area is not significantly modified by low amount of gold or nitrogen.

Fig. S1 shows the XRD diagrams of TiO_2 LP and *X*–Au–TiO_2 with *X* ranging from 0.04 to 0.16 wt%. The patterns show one major anatase crystalline structure (1 0 1) with corresponding peak at $2\theta = 25.32°$ and traces of rutile as shown by the (1 1 0) peak (small peak at

Table 1
Main synthesis parameters and Gold content of various laser synthesized photocatalysts.

Sample	Ar flow (cm^3/min)	NH_3 flow (cm^3/min)	% Au in the precursor[a]	wt% Au in the powder[b]	wt% N in the powder[b]
TiO_2 LP	1560	0	0	0	0
0.04-Au–TiO_2	1560	0	0.07	0.04	0
0.09-Au–TiO_2	1560	0	0.17	0.09	0
0.12-Au–TiO_2	1560	0	0.24	0.12	0
0.16-Au–TiO_2	1560	0	1.22	0.16	0
N-TiO_2	1460	106	0	0	<0.1
Au/N-TiO_2	1460	58	0.27	<0.05	<0.1

[a] Calculated in the initial precursors mixture.
[b] Determined by inductively coupled plasma optical emission spectrometry (ICP).

Table 2
Nitrogen adsorption analysis and average particle sizes of laser synthesized photocatalysts.

Sample	Specific surface area (m^2/g)$^a_{BET}$	Size (nm)[b]	TEM diameter (nm)	Crystallite size (nm)[c]
TiO_2 LP	159	10.0	6.5 ± 1.40	7.6
0.04-Au–TiO_2	177	9.0	7.4 ± 1.42	7.0
0.09-Au–TiO_2	167	9.5	7.8 ± 1.35	7.0
0.12-Au–TiO_2	163	10.0	8.5 ± 1.8	7.0
0.16-Au–TiO_2	161	9.5	7.0 ± 1.60	7.0
N-TiO_2	162	9.5	8.7 ± 2.66	8.0
Au/N-TiO_2	210	7.5	7.2 ± 1.49	7.0

$2\theta = 27.45^\circ$). Diffraction peak of metallic Au or gold oxide were not observed, this absence can be explained both by the low gold amount below the instrument detection limit and the small size of gold NPs (less than 5 nm) well dispersed on the TiO_2 surface. Fig. S2 presents the XRD diagrams of the Au/N-TiO_2 sample with reference samples (TiO_2 LP, Au–TiO_2, and N-TiO_2) synthesized in similar experimental conditions (except the precursor mixture). Once again, the main crystallographic phase is anatase (peak at $2\theta = 25.32^\circ$). The crystalline structure is not modified compared to TiO_2 LP when N or Au are introduced in the experiment. The average crystallite sizes calculated using the Scherrer equation by the full width at half-maximum of the (1 0 1) diffraction peak of TiO_2, are presented in Table 2.

3.2.2. Chemical analysis

Table 1 shows the gold and nitrogen amounts introduced in the reactive mixture and those measured by ICP in the samples. Fig. 3 shows the evolution of Au amount in the powder in the *X*–Au–TiO_2 samples as a function of the introduced amount in the reactive mixture. At low Au content, the slope shows a linear increase of the Au content in the powder when increasing the gold content of the precursor, proving a good relationship between experimental conditions and final chemical composition. At the highest Au value, the weight of gold in the solution prevents efficient transfer in the droplets and therefore limits the total amount of incorporated gold in the TiO_2 NPs. Compared to wet chemistry, our method allows achieving smaller gold content (for example 0.16 wt% maximum using LP, 2.5% by deposition/precipitation [41], 8% by impregnation [42]). In the co-doped Au/N-TiO_2 and 0.12-Au–TiO_2 samples, the gold content in the precursor was similar but the incorporation of gold is totally different: it was not possible to detect gold presence by ICP in the co-doped sample. This effect can be related only to the presence of NH_3, even in very low gas flow, certainly modifying the chemistry in the reaction zone by the addition of this reducing agent.

3.2.3. Optical properties

Fig. 4 shows the UV–vis diffuse reflectance spectra of TiO_2 LP, *X*–Au–TiO_2 with *X* from 0.04 to 0.16 wt% (Fig. 4A) and TiO_2 LP, N-TiO_2, Au/N-TiO_2, (Fig. 4B). The band gap of all powders are calculated according to the transformed Kubelka–Munk function *vs* the energy of light [43]. In the case of *X*–Au–TiO_2 samples (Fig. 4A), there is no influence of gold on the band gap energy of TiO_2 (3.1 eV). All Au–TiO_2 NPs present a wide absorbance band in the visible range, from 500 to 800 nm, with a maximum centered at 620 nm. Its intensity slightly increases in correlation with increasing gold content. This band is usually assigned to the plasmon resonance of gold nanoparticles [30]. In the frame of the Mie theory, for spherical particles of small size compared to the wavelength λ, the absorption cross section of a single nanoparticle embedded in a homogeneous medium is $(C_{abs} = 8\pi^2 n_m^3 a/\lambda)\mathrm{I\,m}((n^2 - n_m^2)/(n^2 + n_m^2))$ [44], where Im() stands for imaginary part, *a* corresponds to the

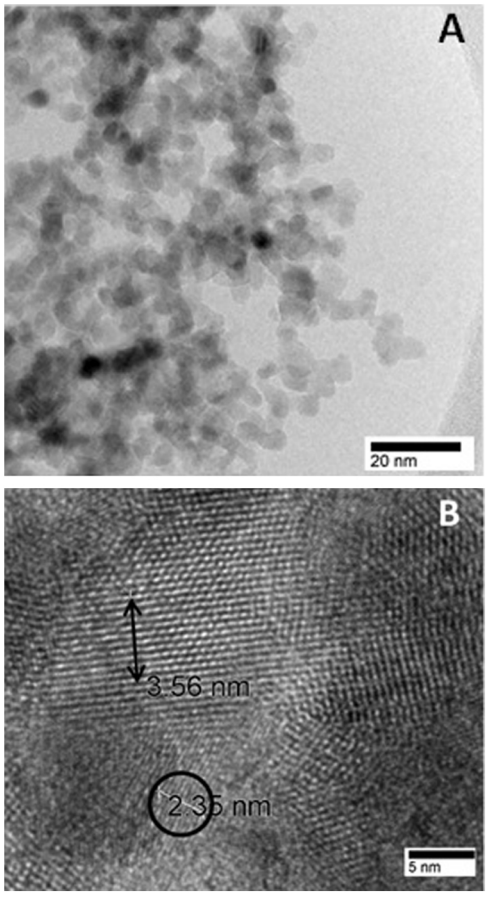

Fig. 2. A. Typical TEM picture of 0.16-Au–TiO_2 sample. B. HRTEM pictures of 0.16-Au–TiO_2 sample where Au and TiO_2 crystallites are pointed.

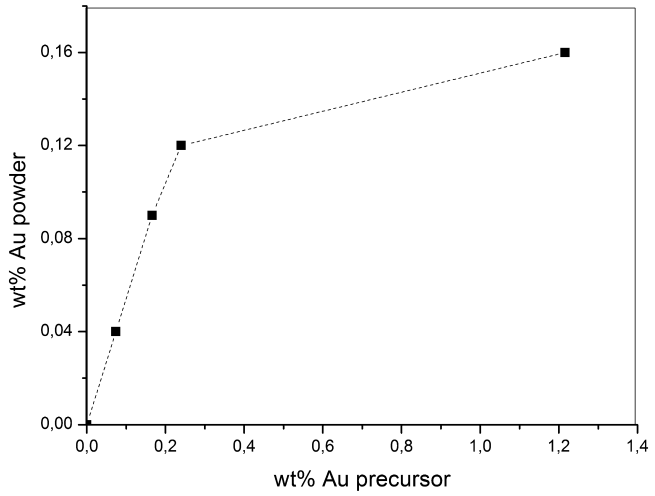

Fig. 3. Evolution of Au wt% in the NPs as a function of Au content in the precursor mixture.

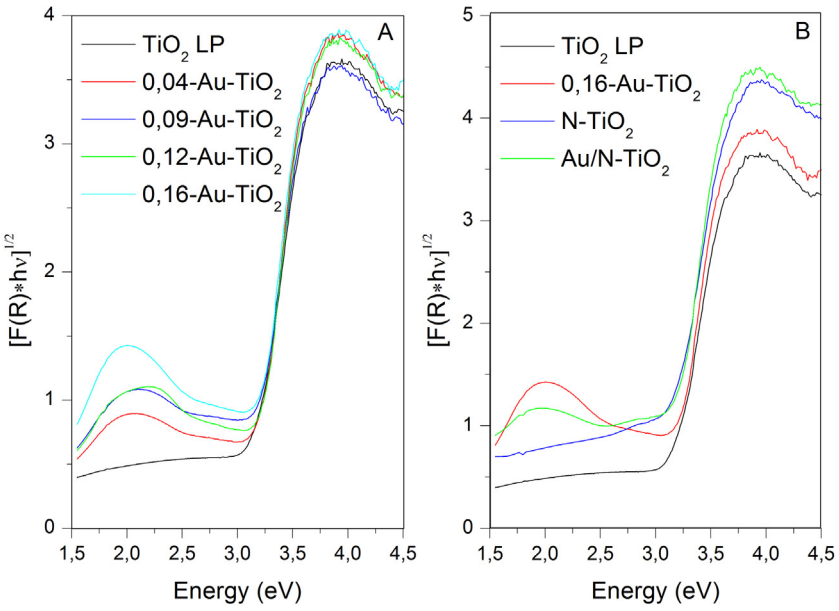

Fig. 4. Transformed Kubelka–Munk (from diffuse reflectance spectra) function vs energy of the excitation source of laser synthesized photocatalysts. Determination of the optical band gap is performed by reference to the indirect gap in semiconductors [43].

particle radius, n and n_m correspond to the complex refractive indices of, respectively, the particle and the medium. The expression is valid when $(2\pi/\lambda)n_m a \ll 1$ and then for Au particles of 2–3 nm diameter. The dispersion of the refractive indices defines the wavelength dependence of the plasmon absorption band. Assuming gold nanoparticles in interaction with TiO_2, the Mie theory leads to a plasmon resonance around 2 eV, which is fully consistent with the measurements. The influence of the medium, especially TiO_2, has been observed in several studies [41,45,46].

Fig. 4B, shows that even if the Au and nitrogen amounts are below ICP detection limit, their typical signatures are observable in the UV spectra of N-TiO_2 and Au/N-TiO_2 samples. In this Figure, the plasmon band due to the presence of Au is clearly detected in the Au/N-TiO_2 sample as reported in a previous study [33]. In both N-TiO_2 and Au–N-TiO_2 samples, the absorption band attributed to the presence of nitrogen is located in the visible region between 400 and 485 nm and the optical gap is shifted toward lower energy [27]. This effect is attributed to new energy levels in the electronic band structure of TiO_2 caused by the presence of nitrogen in the TiO_2 lattice, the evolution of this absorption band when the structure evolves from TiO to N-TiO_2 has been studied in detail in a previous study [47]. Nitrogen localization was studied by XPS, Fig. S3 shows that N is mainly located as interstitial atom on Ti—O—N bonds.

3.2.4. Photoluminescence study

Photoluminescence (PL) spectroscopy is widely used to investigate the electron–hole fate in semiconductor particles [48] and is therefore, highly relevant to monitor the electronic interactions between Au and semi-conducting TiO_2 nanocrystals. Fig. 5 shows the PL spectra of samples TiO_2 and Au-loaded TiO_2. All spectra are normalized with regard to the free exciton emission peak of anatase at 3.15 eV (see Supporting information for experimental details and complementary photoluminescence spectra, Fig. S4), allowing a direct comparison of the intensities of the sub-band gap contributions.

PL contributions below the optical band gap are generally associated with electron–hole recombination mechanisms occurring in the presence of electronic defects [49,50]. In our case, a clear contribution at 2 eV is visible for pure TiO_2 as well as for Au-loaded TiO_2 NPs. This feature can be attributed to interfacial self-trapped electrons [51] which are thus found to be dependent on the local environment of the particles. We observe a slight but significant decrease of this feature for sample Au–TiO_2 compared to pure TiO_2. This observation is consistent with reduced radiative recombination of photo-induced electrons trapped at the TiO_2 particle surface. This indicates that efficient charge transfers to the gold can occur. Such observations suggest that our one step process is highly favorable to achieve efficient electronic interactions between the two components. These analyses show that the synthesized Au–TiO_2 samples exhibit improved physical properties, highly suitable for efficient photocatalysts.

3.3. Photocatalytic activity

3.3.1. Adsorption studies

The pollutant adsorption at the catalyst surface is the initial and primordial step prior to the photocatalytic reaction. Therefore,

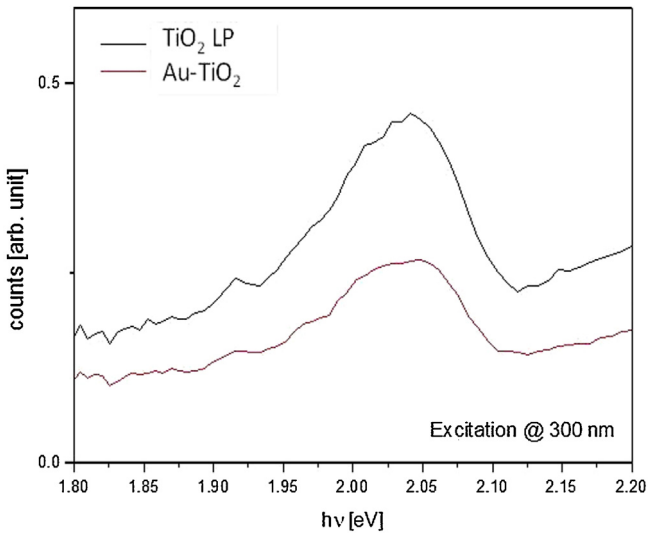

Fig. 5. Photoluminescence (PL) spectra of TiO_2 and Au-TiO_2 nanoparticles.

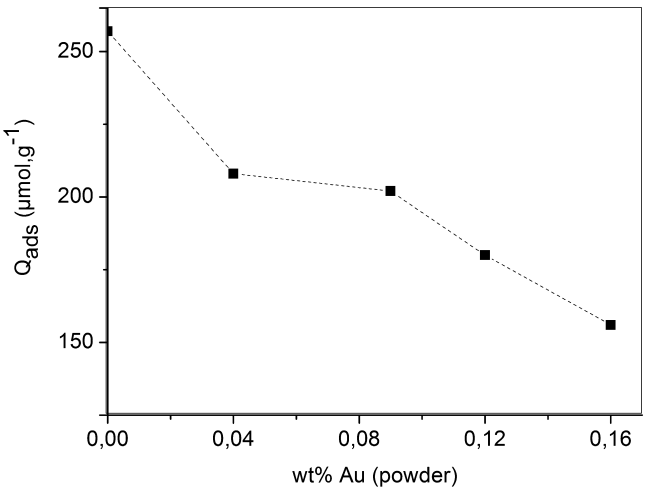

Fig. 6. Adsorbed quantity of FA (Q_{ads}) as a function of different amounts of Au.

the first investigation was the determination of the amount of FA adsorbed on different catalysts under dark condition.

• Reference NPs: TiO_2 LP and P25

The evolution of the amount of formic acid adsorbed in the dark on TiO_2 LP and P25 catalysts is reported in Fig. S5 as a function of time. The maximal FA quantity adsorbed in the dark by TiO_2 LP (257 µmol g^{-1}) is about 3 times higher than this one adsorbed on P25 (87 µmol g^{-1}). This result is directly related to the specific surface area of TiO_2 LP which is three times larger for TiO_2 LP NPs than P25 NPs (see inset Fig. S5).

• *X*–Au–TiO_2 samples

The amount of formic acid adsorbed in the dark per gram of photocatalyst was also studied on *X*–Au–TiO_2 samples (Fig. 6). FA adsorption decreases with increasing Au amount. These results may indicate that some adsorption sites are blocked by gold as suggested in the literature [33,35].

3.3.2. *Photocatalytic degradation of FA: effect of gold under UV irradiation*

• Reference NPs: TiO_2 LP and P25

First of all, it was experimentally verified that direct photolysis of the FA is negligible under UV irradiation alone in agreement with its light absorption properties. Secondly, before irradiation, the FA solution containing the photocatalysts was stirred in the dark until reaching adsorption–desorption equilibrium. Taking into account negligible photolysis and the FA adsorbed under dark, the disappearance observed in the presence of TiO_2 nanomaterials under UV-A conditions is only due to the photocatalytic process. Fig. 7 shows the evolution of the concentration of FA under UV light. TiO_2 LP is about three times more efficient than P25 commonly used as reference in the literature. Actually, the disappearance rate is about 58 µmol L^{-1} min^{-1} for TiO_2 LP and 20 µmol L^{-1} min^{-1} for TiO_2 P25 leading to a total disappearance of FA after 30 min for TiO_2 LP and 60 min for TiO_2 P25. From this result the best efficiency is achieved with the TiO_2 samples exhibiting the highest adsorption as discussed previously (see inset of Fig. 7). This relation may indicate easier surface reactions with increasing adsorption leading to faster degradation rates.

• X–Au–TiO2 samples

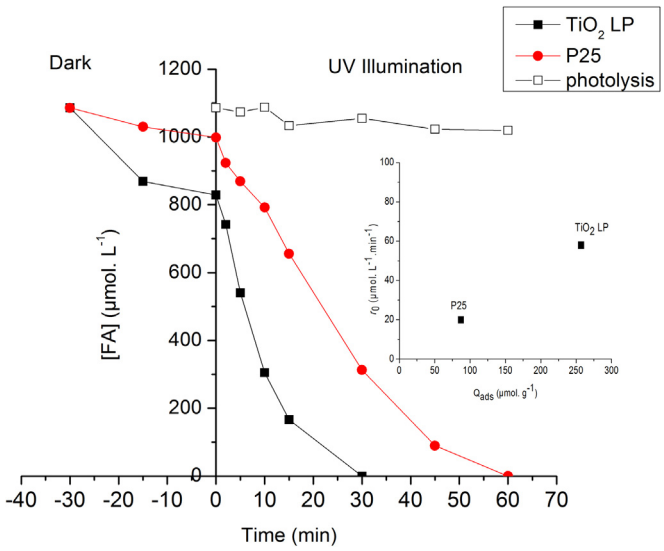

Fig. 7. Photodegradation of formic acid in the presence of TiO_2 LP and P25 under UV illumination. Insert: initial rate disappearance of FA as a function of amount of FA adsorbed.

Fig. 8 shows the photocatalytic disappearance rate of FA as a function of the of Au content. All samples exhibit a higher activity compared to TiO_2 LP (itself more efficient than P25). Contrary to the TiO_2 case, the Au-loaded samples show a decreasing adsorption of FA while the initial disappearance rate slightly increases. This decrease in adsorption is correlated to an increased Au amount as discussed before. The improved efficiency is due to the presence of Au as shown by PL measurements. It indicates that the lowest adsorption is balanced by the improved charge transfer in presence of Au. Dozzi [41] also measures the photocatalytic degradation of FA by Au–TiO_2 photocatalysts with various Au content. He obtained an improved efficiency up to an optimal value of 0.1 to 0.4 wt% followed by a decrease of efficiency when Au is still increased. Our observation of improved efficiency with increasing Au content is in agreement with such results. Moreover, depending on the synthesis method [41], Au NPs were of different sizes. Compared to P25 efficiency, he measured a better activity with the smallest Au NPs, i.e., 2–3 nm in diameter, in good agreement with our results. This improved efficiency is explained by the formation of Schottky barrier at the Au–TiO_2 interface [45], the photogenerated electrons can transfer from CB of TiO_2 to gold NPs leading to an inhibition of electrons holes recombination [52].

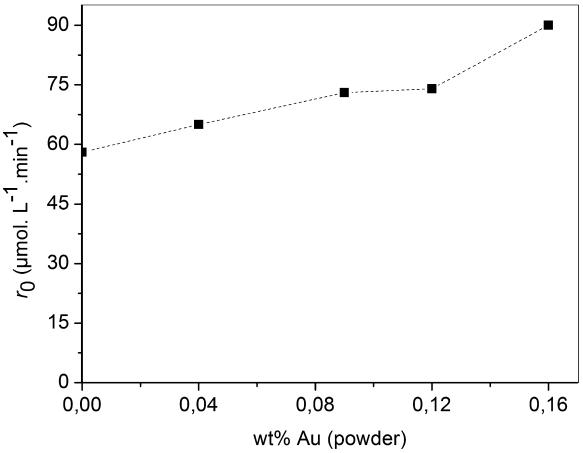

Fig. 8. Evolution of FA initial degradation rate (r_0) as function of different Au amount.

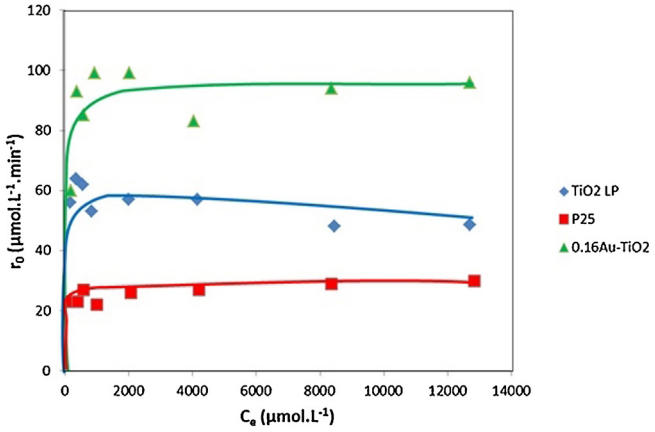

Fig. 9. Initial rates of degradation of FA (r_0) as a function of the concentration of formic acid at the adsorption equilibrium C_e.

• Kinetic study

For a better understanding of the high photocatalytic activity achieved with Au–TiO_2 samples under UV irradiation, the kinetic analysis of the most active sample (0.16-Au–TiO_2) was studied in comparison with TiO_2 P25 and TiO_2 LP. Such study consists of measuring the initial rate of degradation (r_0) as a function of initial formic acid concentration (C_e) for different initial concentrations of FA. Fig. 9 shows that the initial disappearance rates r_0 for FA photodegradation increases rapidly as a function of the C_e concentration, before reaching a plateau. Until a concentration of about 10 ppm ≈ 217 µmol L^{-1} of FA, a first kinetics rate can be suggested (Eq. (1)). Taking into account the increase very important of disappearance rate at low concentration it is not possible to determine K value considering a Langmuir Hinshelwood kinetics. However, it is clear that the rate constant maximal for 0.16-Au–TiO_2 is about twice higher than this one of TiO_2 LP and 4.5 twice higher than this one of TiO_2 P25 for initial concentration higher than 10 ppm.

$$r_0 = kKC_e \quad (1)$$

where r_0 is the initial rate of degradation (µmol L^{-1} min^{-1}), k is the rate constant (µmol L^{-1} min^{-1}), K is the adsorption constant under UV conditions (L $µmol^{-1}$) and C_e is the FA concentration at the adsorption equilibrium (µmol L^{-1}).

The initial degradation rate of 0.16-Au–TiO_2 is higher than for TiO_2 LP and P25. Whatever FA concentration, Au increases the efficiency.

3.3.3. *Photocatalytic degradation of FA: effect of nitrogen and UV and visible irradiation*

• Degradation of FA under UV irradiation

The disappearance of formic acid under UV light irradiation in the presence of P25, TiO_2 LP, N-TiO_2, Au–TiO_2, and Au/N-TiO_2 samples are presented in Fig. 10A showing the adsorption under dark of the reference samples TiO_2 LP and P25 samples together with 0.12-Au–TiO_2, N-TiO_2 and co-doped Au/N-TiO_2 NPs. The three latter samples exhibit similar adsorption after reaching adsorption equilibrium. First of all, we can notice that presence of nitrogen does not affect adsorption of FA. All photocatalysts show better photocatalytic activity than P25. After 45 min of irradiation degradation reaches 100% for all the Laser synthesized samples. Compared with TiO_2 LP, N-TiO_2 appears less efficient under UV irradiation. This observed lower photoactivity is often interpreted in terms of recombination centers especially surface states [53] associated to the presence of Nitrogen. However, few studies concern the degradation of organic compounds under UV light using N-TiO_2 materials and the photocatalytic results are rather dispersed related to the very different photocatalysts materials (various elaboration methods, N amount) as well as choice of pollutants (dye or organic molecule such as TNT (trinitrotoluene)) [54] or oxalic acid [35]. The co- doped Au/N sample shows better activity compared to N-TiO_2, illustrating again the beneficial effect of metallic Au introduction in the samples. Our results appear in good agreement with literature although most studies present data related to decoloration of dyes. Deposition of Au on TiO_2 and N-TiO_2 is an effective way to improve photoactivity for the photodegradation of methyl orange and methylene blue under UV irradiation [32,33]. In the same manner, Daous [54] and Iliev [35] show an increased activity under UV for the destruction of TNT and oxalic acid respectively when Au is added to TiO_2 or N-TiO_2 but does not compare their samples to P25.

• Degradation of FA under visible irradiation

Fig. 10B shows the results concerning the disappearance of formic acid concentration under visible light irradiation for 6 h

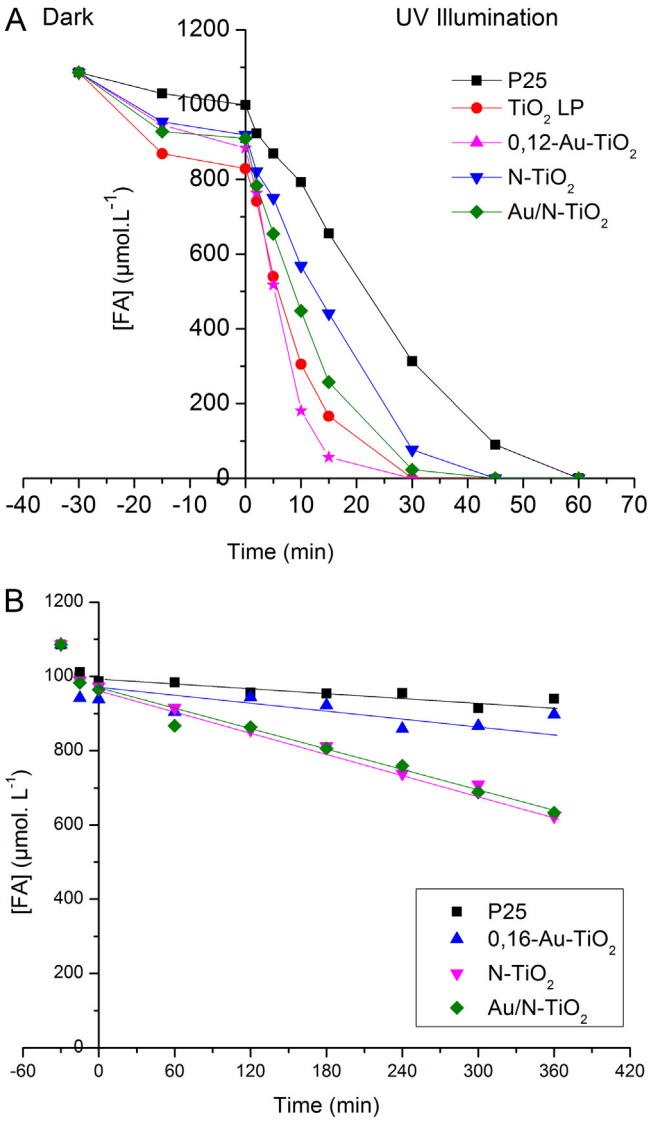

Fig. 10. A. Photodegradation of formic acid with P25, TiO_2 LP, 0.12-Au–TiO_2, N-TiO_2 and Au/N-TiO_2 photocatalysts under UV illumination. B. Evolution of the concentration of formic acid under visible irradiation (400 ≤ λ ≤ 800 nm) over 6 h for P25, 0.16-Au–TiO_2, N-TiO_2 and Au/N-TiO_2.

over the most active sample (0.16-Au–TiO_2), N-TiO_2 and Au/N-TiO_2 compared to the P25 sample. Results show that 0.16-Au–TiO_2 and P25 are similar and do not show any significant photocatalytic activity under visible irradiation. It indicates that although there is some light absorption from the plasmon resonance, there is no energy transfer from the metal to the titania and therefore no photocatalytic activity under visible range. This is in good agreement with Daous and Iliev who observed no activity of their Au–TiO_2 photocatalysts under visible irradiation [35,54]. On the contrary, both N-TiO_2 and Au/N-TiO_2 samples exhibit significant efficiency under visible light (Fig. 10B). Modification with nitrogen is well-known to be active under visible light because of its absorption in the visible region, and also the incorporation of N in the TiO_2 lattice in the form of N—O—Ti and Ti—O—N confirmed by XPS analysis [28]. It leads to a reduction of its band gap energy (~2.1 eV) by introducing localized states above the valence band [27,28]. Au/N-TiO_2 sample exhibits efficiency very similar to N-TiO_2 in the visible range (Fig. 10B), confirming once again that the efficiency under visible is related only to the N doping. This enhancement of the photocatalytic efficiency has been observed by other authors. Indeed, Daous and Iliev observe an activity under visible light only when their TiO_2 and Au–TiO_2 samples contain Nitrogen. Tian et al. also observed much higher activity under visible light for the degradation of 2,4-dichlorophenol with Au/N-TiO_2 and N-TiO_2 photocatalysts compared with TiO_2 or Au-loaded TiO_2 [32].

A detailed explanation about the Au/N-TiO_2 photoactivity is that under visible light two factors are interacting: the first one is the presence of Au nanoparticles on the surface of TiO_2 creating a Schottky barrier at the interface leading to a shift of Fermi level to negative potential; therefore, increase the interfacial charge transfer process. The second is the effect of the incorporation of N, generating new energy levels which decrease the band gap and make easier the electron transfer from the valence band to the conduction band of TiO_2 thus facilitating the transition to Au nanoparticles where electrons are transferred to adsorbed molecules on the TiO_2 surface. The combination of gold and nitrogen decrease the recombination rate of electron/hole pairs and improve the photocatalytic activity under visible light irradiation.

4. Conclusions

In the present work, TiO_2, *X*–Au–TiO_2 (*X* from 0.04 to 0.16 wt%), N-TiO_2 and Au/N-TiO_2 nanoparticles were successfully prepared in one step using a continuous gas phase method, the laser pyrolysis. Using FA degradation as a photocatalytic test, under UV irradiation, all laser-synthesized photocatalysts, including the N-doped TiO_2 samples, present a significant increased photocatalytic activity compared to P25 sample. The efficiency of Au-modified sample is increased when Au content increases. This improvement is attributed to better charge separation in presence of metallic Au. In the case of Au/N-TiO_2 sample, both Au and N are below the detection limit of ICP but significant effect is observed on its photocatalytic activity compared to TiO_2 LP and N-TiO_2. Only N-doped sample present some activity under visible illumination. However, Au/N-TiO_2 sample presenting a better activity than P25 under UV irradiation and significant activity under visible appears a good candidate for further tests with more realistic pollutants.

Acknowledgments

The authors thank Jocelyne Leroy (CEA/SPCSI) for the XPS measurements. The authors would also like to acknowledge New-Indigo program for french-indian support.

Appendix A. Supplementary data

Supplementary data associated with this article can be found, in the online version, at http://dx.doi.org/10.1016/j.apcatb.2015.03.022.

References

[1] N. Serpone, A.V. Emeline, S. Horikoshi, V.N. Kuznetsov, V.K. Ryabchuk, Photochem. Photobiol. Sci. 11 (2012) 1121.
[2] S.J. Teichner, J. Porous Mater. 15 (2008) 311.
[3] X. Chen, S.S. Mao, Chem. Rev. 107 (2007) 2891.
[4] K. Nakata, A. Fujishima, J. Photochem. Photobiol. C Photochem. Rev. 13 (2012) 169.
[5] M.R. Hoffmann, S.T. Martin, W. Choi, D.W. Bahnemannt, Chem. Rev. 95 (1995) 69.
[6] S. Di Mo, W.Y. Ching, Phys. Rev. B 51 (1995) 23.
[7] D. Chatterjee, S. Dasgupta, J. Photochem. Photobiol. C Photochem. Rev. 6 (2005) 186.
[8] S.W. Verbruggen, M. Keulemans, M. Filippousi, D. Flahaut, G. Van Tendeloo, S. Lacombe, J. a. Martens, S. Lenaerts, Appl. Catal. B Environ. 156 (2014) 116.
[9] X. Zhou, G. Liu, J. Yu, W. Fan, J. Mater. Chem. 22 (2012) 21337.
[10] A. Zielińska-Jurek, E. Kowalska, J.W. Sobczak, W. Lisowski, B. Ohtani, A. Zaleska, Appl. Catal. B Environ. 101 (2011) 504.
[11] A. Zielińska-Jurek, J. Hupka, Catal. Today 230 (2014) 181.
[12] P. Wang, B. Huang, Y. Dai, M.-H. Whangbo, Phys. Chem. Chem. Phys. 14 (2012) 9813.
[13] S.K. Ghosh, T. Pal, Chem. Rev. 107 (2007) 4797.
[14] E. Kowalska, O.O.P. Mahaney, R. Abe, B. Ohtani, Phys. Chem. Chem. Phys. 12 (2010) 2344.
[15] A. Dawson, P.V. Kamat, J. Phys. Chem. B 105 (2001) 960.
[16] S.I. Naya, A. Inoue, H. Tada, J. Am. Chem. Soc. 132 (2010) 6292.
[17] W. Hou, W.H. Hung, P. Pavaskar, A. Goeppert, M. Aykol, S.B. Cronin, ACS Catal. 1 (2011) 929.
[18] C.G. Silva, R. Juarez, M. Tiziana, R. Molinari, H. Garcia, J. Am. Chem. Soc. 133 (2011) 595.
[19] V. Jovic, W.-T. Chen, D. Sun-Waterhouse, M.G. Blackford, H. Idriss, G.I.N. Waterhouse, J. Catal. 305 (2013) 307.
[20] J.Z. Zhang, C. Noguez, Plasmonics 3 (2008) 127.
[21] C. Noguez, J. Phys. Chem. C 111 (2007) 3806.
[22] P.K. Jain, X. Huang, I.H. El-Sayed, M. a El-Sayed, Acc. Chem. Res. 41 (2008) 1578.
[23] A. Moores, F. Goettmann, New J. Chem. 30 (2006) 1121.
[24] K.L. Kelly, E. Coronado, L.L. Zhao, G.C. Schatz, J. Phys. Chem. B 107 (2003) 668.
[25] P.A.K. Reddy, P.V.L. Reddy, V.M. Sharma, B. Srinivas, V.D. Kumari, M. Subrahmanyam, J. Water Resour. Prot. 02 (2010) 235.
[26] N.O. Gopal, H.H. Lo, T.F. Ke, C.H. Lee, C.C. Chou, J.D. Wu, S.C. Sheu, S.C. Ke, J. Phys. Chem. C 116 (2012) 16191.
[27] R. Asahi, T. Morikawa, T. Ohwaki, K. Aoki, Y. Taga, Science 293 (2001) 269.
[28] C. Di Valentin, E. Finazzi, G. Pacchioni, A. Selloni, S. Livraghi, M.C. Paganini, E. Giamello, Chem. Phys. 339 (2007) 44.
[29] S. Sato, R. Nakamura, S. Abe, Appl. Catal. A Gen. 284 (2005) 131.
[30] S. Buzby, M.A. Barakat, H. Lin, C. Ni, S.A. Rykov, J.G. Chen, S.I. Shah, J. Vac. Sci. Technol. B 24 (2006) 1210.
[31] G. Shang, H. Fu, S. Yang, T. Xu, Int. J. Photoenergy 2012 (2012) 759306.
[32] B. Tian, C. Li, F. Gu, H. Jiang, Catal. Commun. 10 (2009) 925.
[33] Y. Wu, H. Liu, J.L. Zhang, F. Chen, J. Phys. Chem. C 113 (2009) 14689.
[34] J. Graciani, A. Nambu, J. Evans, J.A. Rodriguez, J.F. Sanz, J. Am. Chem. Soc 130 (2008) 12056.
[35] V. Iliev, D. Tomova, S. Rakovsky, Desalination 260 (2010) 101.
[36] M. Haruta, J. New Mater. Elechtrochem. Syst. 7 (2004) 163.
[37] A. Ayati, A. Ahmadpour, F.F. Bamoharram, M.M. Heravi, H. Rashidi, Chin. J. Catal. 32 (2011) 978.
[38] B. Pignon, H. Maskrot, V. Guyot Ferreol, Y. Leconte, S. Coste, M. Gervais, T. Pouget, C. Reynaud, J.-F. Tranchant, N. Herlin-Boime, Eur. J. Inorg. Chem. 6 (2008) 883.
[39] E. Figgemeier, W. Kylberg, E. Constable, M. Scarisoreanu, R. Alexandrescu, I. Morjan, I. Soare, R. Birjega, E. Popovici, C. Fleaca, L. Gavrila-Florescu, G. Prodan, Appl. Surf. Sci. 254 (2007) 1037.
[40] L. Davydov, P.G. Smirniotis, J. Catal. 191 (2000) 105.
[41] M.V. Dozzi, L. Prati, P. Canton, E. Selli, Phys. Chem. Chem. Phys. 11 (2009) 7171.
[42] A. Ayati, A. Ahmadpour, F.F. Bamoharram, B. Tanhaei, M. Mänttäri, M. Sillanpää, Chemosphere 107 (2014) 163.
[43] E.L. Simmons, App. Opt. 14 (1975) 1380.
[44] C.F. Bohren, D.R. Huffman, Absorption and Scattering of Light by Small Particles, Wiley, 1998.
[45] J. Fang, S.-W. Cao, Z. Wang, M.M. Shahjamali, S.C.J. Loo, J. Barber, C. Xue, Int. J. Hydrogen Energy 37 (2012) 17853.
[46] Y. Borensztein, L. Delannoy, R.G. Barrera, C. Louis, Eur. Phys. J. D 63 (2011) 235.
[47] P. Simon, B. Pignon, B. Miao, S. Coste-Leconte, Y. Leconte, S. Marguet, P. Jegou, B. Bouchet-Fabre, C. Reynaud, N. Herlin-Boime, Chem. Mater. 22 (2010) 3704.
[48] J.G. Yu, H.G. Yu, B. Cheng, X. Zhao, J.C. Yu, W. Ho, J. Phys. Chem B. 107 (2003) 13871.

[49] L. Kernazhitsky, V. Shymanovska, T. Gavrilka, V. Naumov, L. Fedorenko, V. Kshnyakin, J. Baran, J. Lumin. 146 (2014) 199.
[50] V. Melnyk, V. Shymanovska, G. Puchkovska, T. Bezrodna, G. Klishevich, J. Mol. Struct. 744 (2005) 573.
[51] K. Fujihara, S. Izumi, T. Ohno, M. Matsumura, J. Photochem. Photobiol. A 132 (2000) 99.
[52] A. Bumajdad, M. Madkour, Phys. Chem. Chem. Phys. 16 (2014) 7146.
[53] C. Di Valentin, G. Pacchioni, A. Selloni, S. Livraghi, V.R. Cozzi, J. Phys. Chem. B 109 (2005) 11414.
[54] M. Daous, V. Iliev, L. Petrov, J. Mol. Catal. A 392 (2014) 194.